

# Numerical study on accumulated deformation of laterally loaded monopiles used by offshore wind turbine

Min Yang<sup>1</sup> · Ruping Luo<sup>1</sup> · Weichao Li<sup>1</sup> 

Received: 31 December 2016 / Accepted: 28 July 2017 / Published online: 18 August 2017  
© Springer-Verlag GmbH Germany 2017

**Abstract** The design of an offshore monopile is generally governed by its accumulated response to lateral cyclic load, e.g., loads induced by winds and waves. In order to investigate the characteristic of this accumulated response, a user subroutine of degradation stiffness model (DSM) is developed and incorporated into a commercial finite difference program. Based on this program, the effect of load character, pile embedded length, and load eccentricity on the displacement development of monopile is quantified, and the applicability and reliability of the two most used models, power function model, and logarithmic function model, for the prediction of accumulated pile displacement are evaluated. Based on the numerical results, a design model which accounts for the influence of number of loading cycles, load amplitudes, and pile embedded length on the accumulated pile displacement is proposed. The proposed design model is validated against measurements from the field test on scaled monopile driven in dense sand deposit, which proves the validity of the recommended design in this paper.

**Keywords** Monopile · Lateral loading · Accumulated response · Numerical modeling

## Introduction

As a much more feasible and efficient solution to climate change and the limitation of fossil resources, clean and renewable wind energy has been explored extensively in recent years. To gain much stronger and more stable wind resources, many wind farms have been constructed or planned offshore. Current practice shows that monopile foundation has obvious advantages for sites with water depth up to 35 m. The monopile foundation consists of an open-ended steel pipe with an outer diameter  $D$  generally ranging from 3.5 to 8 m, and is driven into the seabed with an embedded length  $L_{em}$  of  $(5\sim 12)D$ . Compared with pile foundations commonly used in the offshore oil/gas platforms with size less than 2 m in diameter and lateral load as 10~20% of vertical load, monopiles have a larger diameter and smaller aspect ratio ( $= L_{em}/D$ ), and are subjected to much higher lateral loading (75~150% vertical load) and overturning moment due to the large height (often up to 100 m) of wind tower. The wind and wave induced cyclic loading has two crucial effects on the structures: the lateral deformation exceeds the limit of a working wind turbine (Achmus et al. 2009) and structure frequency changes, which has big potential for resonance (Leblanc et al. 2010).

To predict the cyclic response of a laterally loaded monopile, many models have been proposed, which may generally be cataloged into the soil resistance/stiffness degradation (SRD) method and pile deformation accumulation (PDA) method. Both methods are commonly based on the design models for monopiles subjected to static loading. To account for the cyclic effect, the SRD method reduces the soil reaction or stiffness from a value determined for monopiles subjected to static/monotonic loading (e.g., Reese et al. (1974) and Garnier (2013)), while the PDA method increases the value of pile deformation predicted for monopiles subjected to static

---

✉ Weichao Li  
WeichaoLI@tongji.edu.cn

Min Yang  
YangMin@tongji.edu.cn

Ruping Luo  
Luo.Ruping@outlook.com

<sup>1</sup> Department of Geotechnical Engineering, Tongji University, 1239 Siping Road, Shanghai 200092, People's Republic of China

loading by a coefficient larger than 1 (e.g., Peralta (2010) and Li et al. (2015)). Even though the SRD method is recommended by API (2011) and DNV (2014), both methods are widely adopted to predict the accumulated pile displacement under cyclic lateral loading (e.g., Little and Briaud (1988), Rajashree and Sundaravadivelu (1996), Dewaikar et al. (2008), Leblanc et al. (2010), Klinkvort and Hededal (2013), Carswell et al. (2016)).

For its simplicity and success in design of offshore oil/gas platform, the  $P$ - $y$  curve method, in which a beam is used to represent the pile, and the ground soil is modeled as discrete independent nonlinear springs, is recommended for design of laterally loaded monopiles in current standards/guidelines, e.g., API (2011) and DNV (2014). For the cyclic loading design, both API and DNV recommend that the soil reaction  $P$  is reduced from a value determined for piles subjected to static/monotonic loading to account for the cyclic effect, which may be named as soil stiffness/resistance degradation method. This reduction of soil reaction is independent of the load-unload cycle numbers, which leads the predicted displacement to a constant value for a cyclically loaded pile/monopile. However, this is in contrast with the field observations, e.g., Long and Vanneste (1994) and Li et al. (2015), in which the accumulated displacement is heavily dependent on the cycle numbers, load amplitudes, pile embedded length and so on. With regard to the PDA method, mainly there are two mathematic models employed to predict the accumulated response of monopiles, i.e., power function model and logarithmic function model, see Eqs. (1) and (2), (e.g., Verdure et al. (2003), Leblanc et al. (2010), Bienen et al. (2012), Klinkvort and Hededal (2013)), where  $\alpha$  and  $b$  are model parameters. However, the applicability and feasibility of both widely used models are not well evaluated. Additionally, the effect of monopile geometry and load conditions on the value of model parameter is not fully studied.

$$y_N = y_1 N^\alpha \quad (1)$$

$$y_N = y_1 (1 + b \ln(N)) \quad (2)$$

Based on the degradation stiffness model (DSM) proposed by Achmus et al. (2009), this paper investigates the long term cyclic behavior of laterally loaded monopile foundations through three dimensional finite difference models. The feasibility of power function model and logarithmic function model in predicting the cyclic accumulated monopile displacement is examined, and then recommendation is given for determination of power model parameter  $\alpha$ . The effect of monopile embedded length, load eccentricity, and load amplitudes are incorporated in the correlations to determine the power model parameter. Finally, measurement from cyclic loading test on a scaled monopile is employed to validate the recommended design in this paper.

## Numerical modeling

### Site description

In this study, a test site reported by Li et al. (2015) is adopted mainly for three reasons: 1) this site consists of over-consolidated dense sand deposit which is comparable to dense sands at North Sea where many wind turbines have been or will be installed; 2) series of pile loading tests, especially the cyclic test on scaled monopile loaded laterally with up to 5000 cycles, were performed (e.g., Li et al. (2015) and Kirwan (2015)); 3) the ground condition and soils at this site have been well investigated by performing a series of laboratory tests and in-situ testing, e.g., Tolooiyan and Gavin (2011). A general description of this site is given below.

This site is a uniform, fine sand deposit (containing 5~15% of clay and silt size particles) with a relative density close to 100%. The soil unit weight is relatively constant with a depth value of 20 kN/m<sup>3</sup> and the depth of water table is about 15 m below mudline. Triaxial compression tests give the peak friction angle  $\phi_p = 54^\circ$  at 1 m depth down to  $42^\circ$  at about 5 m depth and the constant volume friction angle,  $\phi_{cv}$  is  $37^\circ$  regardless of depth.

### Constitutive models

The ground soil of this site is modeled as an elasto-plastic material with Mohr-Coulomb (MC) failure criterion, which has been successfully employed to study the dimension effect of a laterally loaded monopile by Yang et al. (2016). The values of model parameters are summarized in Table 1. Since this site consists of over-consolidated, dense sand deposit, the ground is subdivided into four thin layers to account for the variation of soil strength and stiffness at shallow depth. The dilatancy angle in Table 1 is determined according to Bolton (1986).

Monopiles are modeled as a linear elastic, solid cylinder with an equivalent bending stiffness of the hollow steel pipe piles, which has Young's modulus of 210 GPa and Poisson's ratio of 0.2.

### Degradation stiffness model

To numerically model the cyclic response of monopiles, Achmus et al. (2009) proposed the degradation stiffness model (DSM) to predict the accumulated response of monopiles subjected to lateral loading, which is able to account for the number and amplitude of cyclic loading. The parameters in DSM could be conveniently determined from the result of cyclic triaxial test and this model has been widely used for its numerical accuracy and computation efficiency, e.g., Depina et al. (2015). Therefore, in this study, the DSM is incorporated into the finite difference program to model the

**Table 1** Model parameters for ground soil

Layer No	Depth, $z$ (m)	Friction angle, $\phi_p$ (°)	Dilatancy angle, $\psi$ (°)	Cohesion strength, $c$ (kPa)	Secant elastic module, $E_s$ (MPa)	Poisson's ratio, $\nu$	Unit weight, $\gamma$ (kN/m <sup>3</sup> )
1	0 ~ 1	55.5	23.1	1	26.5	0.2	20
2	1 ~ 2	52.5	19.4	1	39.8	0.2	20
3	2 ~ 3	49.5	15.6	1	45.0	0.2	20
4	3 ~ 3.5	47.3	12.8	1	47.0	0.2	20
5	3.5~	42	6.3	1	50.0	0.2	20

accumulated response of monopile subjected to lateral loading. A general description of the DSM is made below and details are given in the literature (Achmus et al. 2009, Kuo et al. 2012).

Figure 1 illustrates the stress-strain relationship of a soil sample in a cyclic triaxial test with constant stress amplitude, where  $E_{s,1}$  and  $E_{s,N}$  are the secant stiffness corresponding to the 1st and  $N^{\text{th}}$  load cycles,  $\varepsilon_{e,1}^a$  and  $\varepsilon_{e,N}^a$  are the axial elastic, and  $\varepsilon_{p,1}^a$  and  $\varepsilon_{p,N}^a$  the axial plastic strain corresponding to 1<sup>st</sup> and  $N^{\text{th}}$  load cycles, respectively. Assuming the elastic axial strain  $\varepsilon_e^a$  to be negligible, the DSM model links soil's secant stiffness  $E_s$  and accumulated plastic axial strain  $\varepsilon_p^a$  (Achmus et al. 2009) according to the Eq. (3):

$$\frac{E_{s,N}}{E_{s,1}} = \frac{\varepsilon_{e,1}^a + \varepsilon_{p,1}^a}{\varepsilon_{e,N}^a + \varepsilon_{p,N}^a} \approx \frac{\varepsilon_{p,1}^a}{\varepsilon_{p,N}^a} \tag{3}$$

To predict the accumulated plastic strain  $\varepsilon_{p,N}^a$  in a cyclic triaxial test, Achmus et al. (2009) adopted a semi-empirical formula (Huurman 1996), with which the degradation of secant stiffness can be expressed with Eq. (4):

$$\frac{E_{s,N}}{E_{s,1}} = \frac{\varepsilon_{p,1}^a}{\varepsilon_{p,N}^a} = N^{-b_1(X)^{b_2}} \tag{4}$$

Where  $b_1$  and  $b_2$  are material constants,  $X$  is the cyclic stress ratio and equal to the ratio of the major principal stress at static failure state  $\sigma_{1,sf}$  to the major principal stress for the cyclic stress state under consideration. Achmus et al. (2009) suggested that, for dense sand the values of  $b_1$  and  $b_2$  are 0.20 and 5.76, respectively. For the soil element around a laterally loaded monopile, to eliminate the influence of geostatic stress on the development of soil accumulated cyclic strain, a characteristic cyclic stress ratio  $X_c$  is introduced by Achmus et al. (2009) and defined as Eq. (5):

$$X_c = \frac{X^{(1)} - X^{(0)}}{1 - X^{(0)}} \tag{5}$$

In Eq. (5), the index <sup>(1)</sup> means the cyclic stress ratio at loading phase and the index <sup>(0)</sup> means at unloading phase.

**Numerical model verification**

To evaluate the validity of DSM, the cyclic response of scaled monopile PC2 (Li et al. 2015) is modeled. Test monopile PC2 has an outer diameter  $D$  of 0.34 m, embedded length  $L_{em}$  of 2.2 m, and bending stiffness of 39,000 kN.m<sup>2</sup>. The one-way, multi-amplitudes cyclic loading was applied at a height  $L_{up}$  of 0.4 m above the ground level. The values of soil model parameters are summarized in Table 1. For each soil layer, the values of  $b_1$  and  $b_2$  in Eq. (4) are 0.20 and 5.76, respectively (Achmus et al. 2009). The secant modulus  $E_s$  of the soil is varied with mean stress level. In Table 1, the site is divided into five layers, and the mean stress of each layer is calculated, then the secant modulus  $E_s$  in each layer can be estimated by referring to the laboratory results given by Tolooiyan and Gavin (2011). For simplification and numerical efficiency, a half symmetrical model is adopted in this study. The elastic modulus of the solid monopile  $E_p$  is calculated based on the equivalence bending stiffness, as follows:

$$E_p \frac{\pi D^4}{64} = EI_{p,m} \tag{6}$$

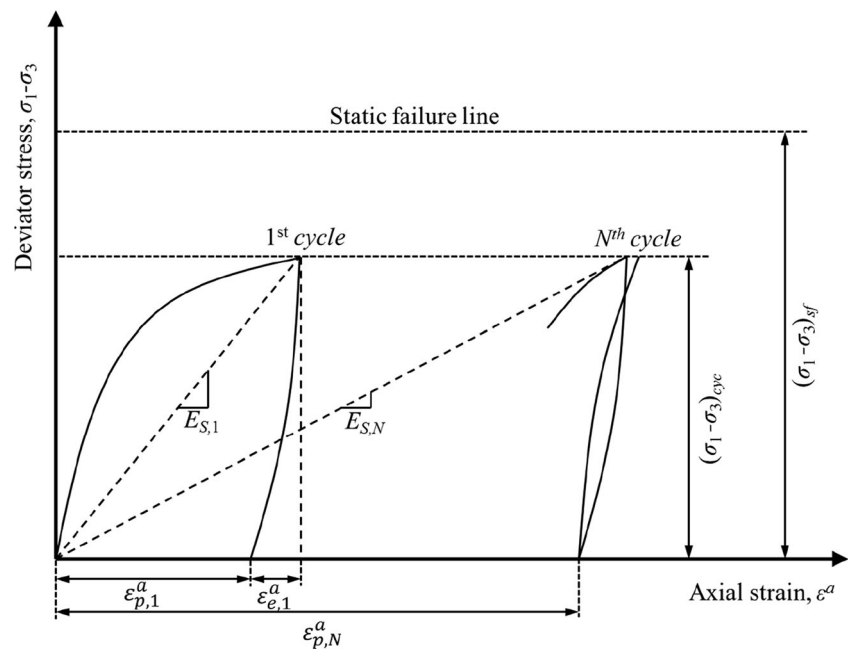
Where:  $E_p$  is the elastic modulus of the solid monopile;  $D$  is monopile outer diameter;

$EI_{p,m}$  is the calibrated bending stiffness of scaled monopile in the field test, = 39,000 kN.m<sup>2</sup> (Li et al. 2013).

According to Achmus et al. (2009), the width of the soil domain  $B$  is set as 4.1 m (=12 $D$ ), the length  $L$  is 8.2 m (=24 $D$ ), and the depth  $H$  is 3.5 m (=10.3 $D$ ). The whole model is represented by 15,664 zones and 17,568 grid-points. An overview of this numerical model is given in Fig. 2.

Two interfaces, the side interface and the bottom interface, are set between the solid monopile and the soil domain to simulate the soil-pile interaction. According to the guidelines of FLAC<sup>3D</sup> user manual, if the material on one side of the interface is much stiffer than on the other, then the appropriate minimum value of shear stiffness  $k_s$  of the interface should be ten times the equivalent stiffness of the soft neighboring zone. In this case, the deformability of the

**Fig. 1** Cyclic response of soil element in triaxial test under constant stress amplitude, modified from Achmus et al. (2009)



whole system is dominated by the soft side. Making the interface stiffness ten times the soft-side stiffness will ensure that the interface has minimal influence on the system compliance. Therefore, the normal and shear stiffness of the interfaces are set to  $10^6$  kPa/m for the two interfaces. The strength parameters of the interfaces elements are taken as  $c = 0$  kPa, friction angle  $\phi = 26^\circ$  and  $24^\circ$  for the side and bottom interface, respectively, which are consistent with those adopted by Yang et al. (2016).

Figure 3 illustrates the comparison of monotonic and cyclic response of monopile between measured and numerically predicted under monotonic loading and cyclic loading under the first load amplitude as termed LA1 of PC2 (Li et al. 2015),

which shows a good agreement and proves the validity of the numerical model adopted by this study.

### Parametric study

To study the accumulated response of monopile under lateral loading, monopiles with diameter of 6 m are modeled. Additionally, the effect of the slenderness ratio  $L_{em}/D$  and load eccentricity  $L_{up}$  is quantified by changing the values of  $L_{em}/D$  and  $L_{up}/D$ . Monopiles with eight geometry dimensions in total are modeled in this study, which are summarized in Table 2. In this study, the slenderness ratio ranges from 3 to 10, and the load eccentricity is from 4 to 15. The geometries investigated

**Fig. 2** Mesh of numerical model

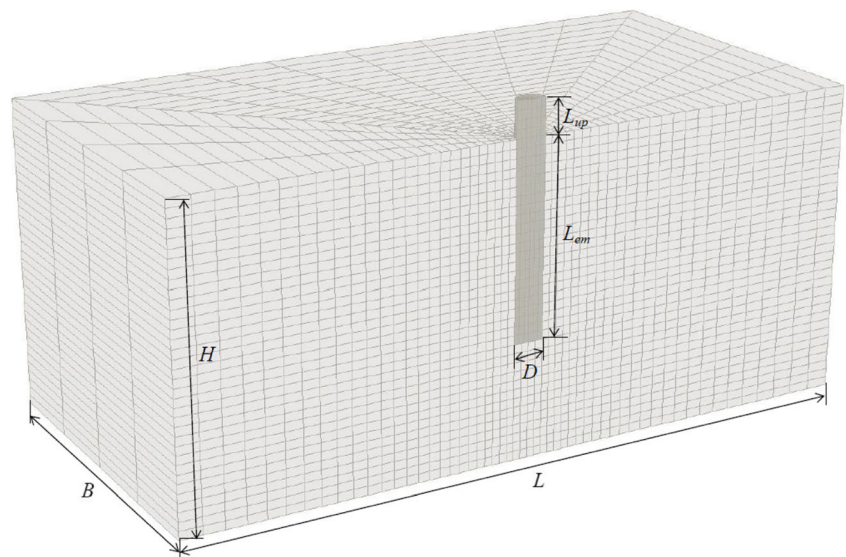
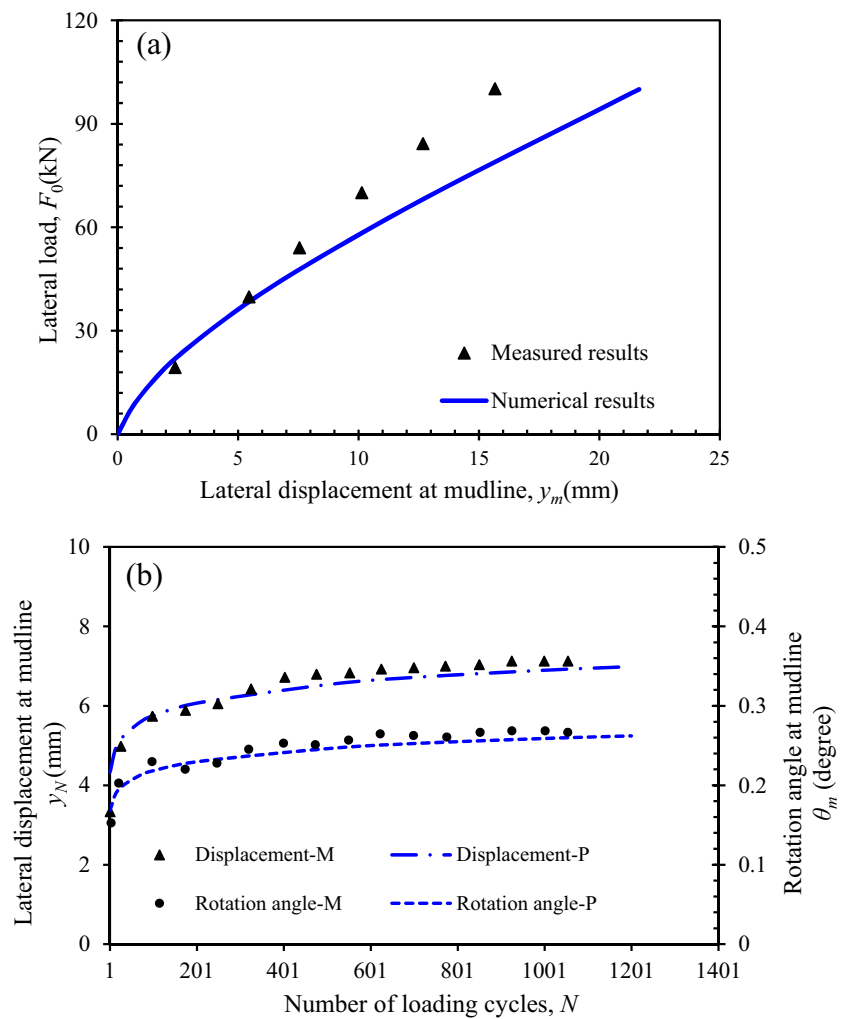


**Fig. 3** Comparison of pile head response of PC2 between measured and numerically predicted. (a) monotonic loading; (b) cyclic loading



in this study cover the representative values for monopiles used in offshore wind farm (Klinkvort and Hededal 2014). According to Leblanc et al. (2010), parameters  $\zeta_b = F_{max}/F_u$ , and  $\zeta_c = F_{min}/F_{max}$ , in which  $F_{max}$  and  $F_{min}$  are the maximum and minimum load applied in each load cycle are introduced to characterize the applied cyclic load, and  $F_u$  is the ultimate load capacity of laterally loaded monopiles. In this study, only  $F_{min} = 0$  kN is considered, that is to say, the value of  $\zeta_c$  is 0. With regard to the ground soil, a uniformed ground is adopted, which has the same properties as those of layer 5 in Table 1. Monopiles simulated in this study experience up to  $6 \times 10^5$  load cycles.

## Results and discussion

### Determination of ultimate load capacity

To determine the ultimate capacity  $F_u$  of laterally loaded monopiles, a number of criteria have been proposed which are mainly based on the monopile head displacement or

rotation, e.g., Zdravković et al. (2015). In this study, a monopile with each geometry dimension is modeled under lateral monotonic loading. For each monopile, ultimate load capacities are determined according to monopile’s displacement and rotation at mudline, i.e.,  $y_0 = 0.1D$ ,  $\theta_0 = 2^\circ$ , see Table 3. A comparison of ultimate capacities corresponding to both criteria is summarized in Table 3 for each monopile. It demonstrates that ultimate capacities determined with criteria of  $y_m = 0.1D$  and  $\theta_m = 2^\circ$  agree with each other well, and it is independent of the slenderness ratio and load eccentricity, which is in line with the observation by Ahmed and Hawlader (2016). In this study, the criterion of  $y_m = 0.1D$  is adopted to determine the ultimate capacity  $F_u$  for each monopile.

A further study on Table 3 shows that: the ultimate load capacities  $F_u$  is increased as the increasing of monopiles’ slenderness ratio, and once monopile’s embedded length is larger than  $8D$ , the increment is obviously smaller. This embedded length is close to the calculated critical length with method recommended by Randolph (1981), which is equal to  $7.2D$  for this case.

**Table 2** Cases in parametric study

Pile No.	Embedded ratio $L_{em}/D$	Load eccentricity $L_{up}/D$	Load parameter, $\zeta_b$	Number of loading cycles, $N$
<i>L3e6</i>	3	6	0.24, 0.41, 0.73	1, 5, 20
<i>L6e6</i>	6		0.28, 0.42, 0.56, 0.69, 0.83, 0.97	50, 100, 200
<i>L8e6</i>	8		0.29, 0.39, 0.49	500, 1000, 2000
			0.59, 0.78	5000, 10,000
<i>L9e6</i>	9		0.36, 0.55, 0.64	30,000, 50,000
			0.73, 0.82, 0.91	100,000, 150,000
<i>L10e6</i>	10		0.35, 0.53, 0.61	300,000, 600,000
			0.70, 0.79, 0.88	
<i>L6e4</i>	6	4	0.26, 0.33, 0.43	
			0.54, 0.65, 0.87	
<i>L6e10</i>		10	0.38, 0.46, 0.58	
			0.77, 0.96	
<i>L6e15</i>		15	0.26, 0.42, 0.53	
			0.63, 0.79	

**Cyclic response**

The accumulated deformation of the monopile with various load amplitudes is analyzed. Figure 4 shows the accumulated monopile head displacement versus number of loading cycles of a monopile *L6e6* ( $L_{em} = 6D, L_{up} = 6D$ ),  $y_N$  is the lateral displacement of the monopile at mudline after  $N_{th}$  load cycles. As shown in Fig. 4 that normalized displacement  $y_N/y_1$  is increased with the increasing of load cycles, and the increasing rate of  $y_N/y_1$  is heavily related to the maximum load applied in each cycle, i.e., related to the value of  $\zeta_b$ . According to Fig. 4, the maximum loading cycles needed to reach a plateau value of accumulated displacement is increased with the increasing of load amplitude. For load amplitude corresponding to  $\zeta_b = 0.28$  and  $0.42$ , the accumulated displacement reaches a plateau when the number of loading cycles is no more than  $10^5$ , while the accumulated displacement cannot converge even after up to  $6 \times 10^5$  loading cycles with load amplitude parameter  $\zeta_b$  larger than a value, e.g.,  $\zeta_b = 0.69$ .

**Depth of rotation point**

Unlike the displacement of long slender piles under lateral loading, the large diameter monopile commonly behaves as a rigid monopile, which rotates around a rotation point located at some depth above the monopile tip. To investigate the depth of rotation point  $z_r$  of monopiles under lateral loading, the rotation depth for different load amplitudes and loading cycles of monopile *L6e6* are plotted in Fig. 5. It shows that, the depth of rotation point increases as the increasing of load cycles, and independent of the magnitude of applied load amplitudes. In general, all rotation points approximately locate at a depth of  $(0.65 \sim 0.75)L_{em}$ , which agrees with that observed from

experimental (Li et al. 2017) and numerical modeling (Ahmed and Hawlader 2016).

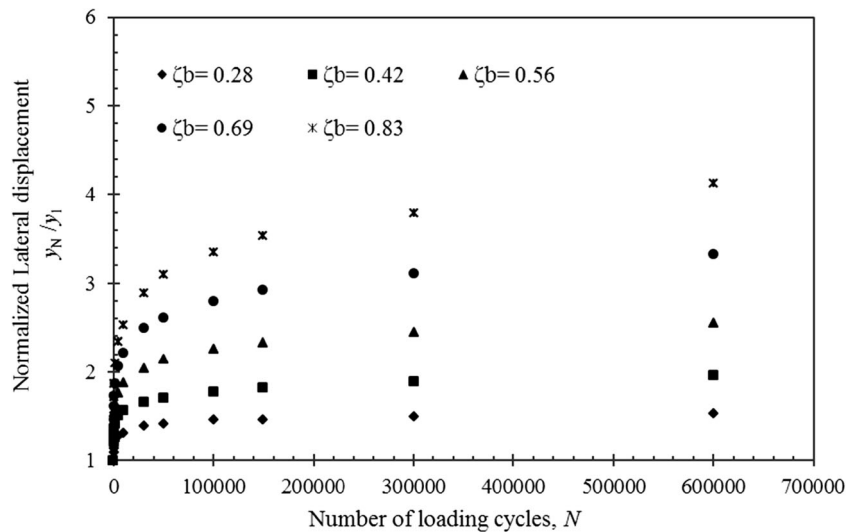
**Comparison between logarithmic and power models**

To study the applicability and reliability of two commonly used models, logarithmic model and power model, for prediction of accumulated monopile head response, accumulated displacement at mudline of each monopile under various load amplitudes is analyzed. Figure 6 shows the accumulated displacement of monopile *L10e6* ( $L_{em} = 10D, L_{up} = 6D$ ) and *L6e15* ( $L_{em} = 6D, L_{up} = 15D$ ), which demonstrate that both models generally model the accumulated response of monopiles well. However, a further study shows that the logarithmic model underestimates the response of a monopile with smaller slenderness ratio and larger load eccentricity condition when the load amplitude is large. For example, as shown in Fig.6 (b), for the monopile with  $L_{em}/D = 6, L_{up}/D = 15, \zeta_b = 0.79$ , the numerical calculated normalized displacement  $y_N/y_1$  is 4.48 when the loading cycle is  $6 \times 10^6$ . The power model gives a prediction of 4.49, while a value of 4.00 is estimated with the logarithmic model.

**Table 3** Ultimate load capacity determined for each monopile

Criteria	Determined ultimate load capacity, $F_u$ (MN)								
	Pile embedded ratio, $L_{em}/D$ ( $L_{up} = 6D$ )				Loading eccentricity, $L_{up}/D$ ( $L_{em} = 6D$ )				
	3	6	8	9	10	4	6	10	15
$y_m = 0.1D$	12.0	35.6	51.7	55.0	57.0	45.7	35.6	26.0	19.0
$\theta_m = 2^\circ$	10.3	37.5	58	61.7	63.7	50.5	37.5	27.3	19.5

**Fig. 4** Accumulated displacement of monopile head ( $D = 6\text{ m}$ ,  $L_{em} = 6D$ ,  $L_{up} = 6D$ )



**Coefficient of power model**

Compared with the logarithmic model, power model shows advantages in simulation of accumulated response of laterally loaded monopiles. Therefore, in the following contents, only power model is considered. To investigate the parameter of power model, the linear regression method is employed and the value of model parameter  $\alpha$  for each case is determined. For monopile L6e6, the value of power model coefficient  $\alpha$  versus load amplitude parameter  $\zeta_b$  is shown in Fig. 7, which demonstrates that the value of  $\alpha$  linearly increases with the increasing of load amplitude. This means that larger load amplitudes lead to a higher rate of displacement accumulating, which is in line with physical modeling results (Leblanc et al. 2010; Klinkvort and Hededal 2013). For each monopile, the derived data sets of  $\alpha$  versus  $\zeta_b$  are fitted with straight line, and since the data sets for monopiles with embedded length of  $8D$  or larger all fall on nearly one

straight line, one line is employed to fit these three data sets, which is illustrated in Fig. 7. A further study on the slopes of these fitted lines shows that: the magnitude of slope decreases from 0.168 to 0.033 as the embedded length of monopile increasing from  $3D$  to  $8D$ , and once the embedded length is larger than  $8D$ , value of model parameter  $\alpha$  only depends on the load parameter  $\zeta_b$ . It can be concluded that once the monopile’s embedded length is larger than its critical length, the value of model parameter  $\alpha$  only depends on the load parameter  $\zeta_b$ .

To investigate the effect of load eccentricity, power model coefficients for monopiles with embedded length of  $6D$  is studied, and the model coefficient versus load parameter is shown in Fig. 8. It can be seen that all the date sets closely fall on a straight line, which demonstrates that the load eccentricity has negligible effect on the model coefficient regardless of the load parameter  $\zeta_b$ .

Therefore, based on the results analyzed above, a general design procedure is recommended for estimation of accumulated response of a monopile:

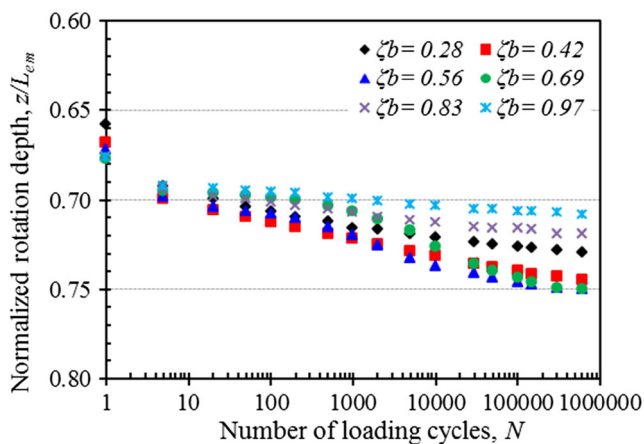


**Fig. 5** Lateral displacement for different load amplitudes and loading cycles

- (a) according to the geometry of monopile and soil condition, the static response of this monopile can be predicted, from which the lateral displacement  $y_1$  corresponding to each magnitude of applied load and the ultimate load capacity  $F_u$  can be estimated.
- (b) based on the environmental load and the ultimate load capacity determined in step (a), the load amplitude parameter  $\zeta_b$  can be calculated.
- (c) based on the monopile’s slenderness ratio  $L_{em}/D$ , and load parameter  $\zeta_b$ , the value of power model parameter  $\alpha$  can be estimated with Fig. 7, since the value of  $\alpha$  is independent of load eccentricity.
- (d) the accumulated deformation  $y_N$  of laterally loaded monopile can be predicted with Eq. (1).

**Fig. 6** Comparison of predictive models for cyclic accumulated displacements: (a)  $L_{em}/D = 10$ ,  $L_{up}/D = 6$ ; (b)  $L_{em}/D = 6$ ,  $L_{up}/D = 15$

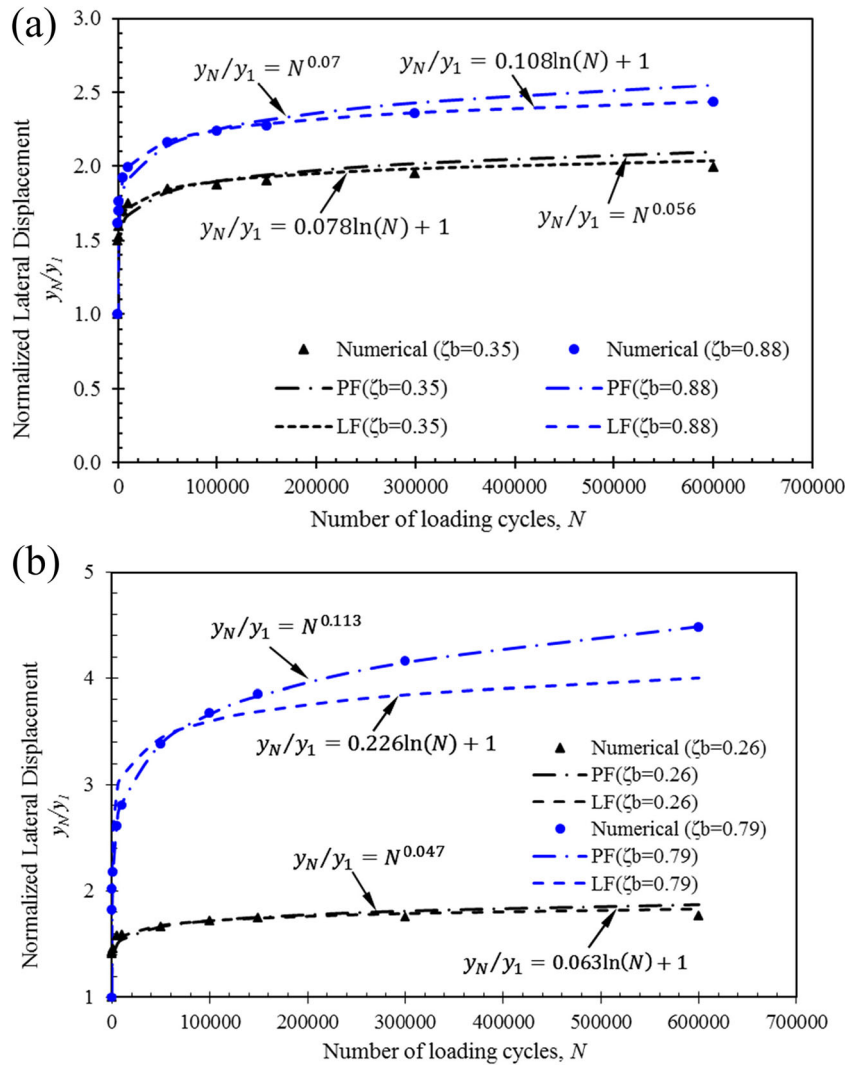


**Fig. 7** Variation of model coefficient with load amplitude for different monopile embedded ratio

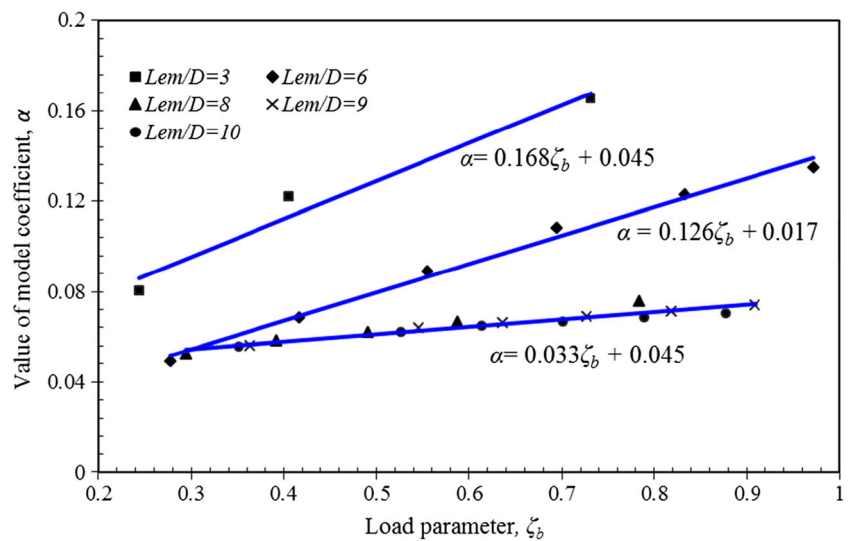
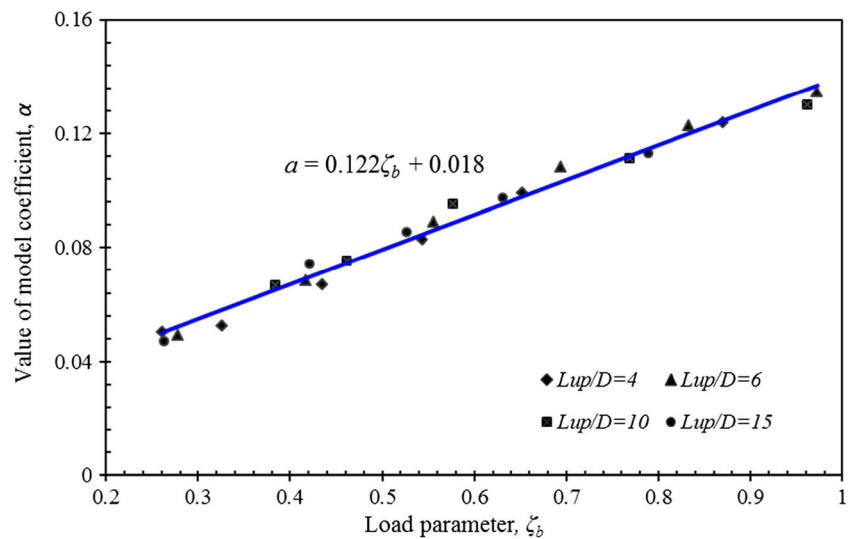




**Fig. 8** Variation of model coefficient with load amplitude for different load eccentricity



**Validation**

To validate the proposed design, measurement from field tests on scaled monopile PC2 driven into dense silica sand is employed (Li et al. 2015). A detailed description on PC2 has been given in the previous section. In addition to the proposed design, models recommended by another four studies (Little and Briaud 1988; Long and Vanneste 1994; Verdure et al. 2003; Bienen et al. 2012) are introduced for comparison of accumulated monopile head displacement, see Fig. 9. The PDA models proposed by Little and Briaud (1988) and Long and Vanneste (1994) are based on the power model, and the other two PDA models are based on the logarithmic model (Verdure et al. 2003; Bienen et al. 2012). The details of these four PDA models are summarized in Table 4.

In general, all these models produce a relatively good prediction with errors around 20% of measured value after 1000 load cycles. This paper’s proposed design model gives a better prediction with an error of 13%, which proves the validity of the proposed design. It should be noted that the PDA model proposed by Little and Briaud (1988) gives a better prediction of accumulative monopile displacement compared to the proposed model of this study, which may be the result of similar loading conditions and monopile dimensions between the validation case and the field test conducted by Little and Briaud (1988). However, the PDA model proposed by Little and Briaud (1988) is independent of the load condition and geometry of the monopile, the effect of which has been incorporated in this study refined model.

**Fig. 9** Comparison of accumulated displacement between measured and predicted with various models

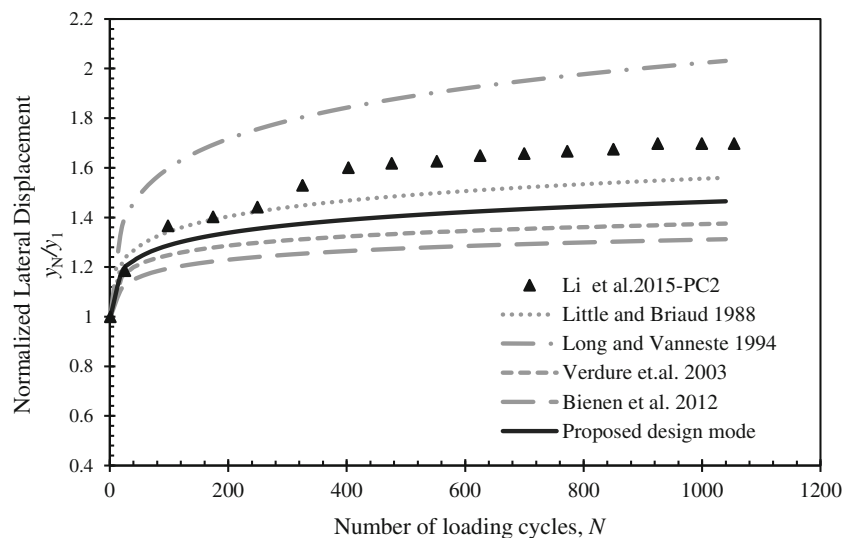


**Table 4** The PDA models used for comparison

Model	Model equation	Reference
PM1	$y_N = y_1 \times N^{0.064}$	Little and Briaud (1988)
PM2	$y_N = y_1 \times N^\alpha$ ; $\alpha = 0.102 \times F_L \times F_I \times F_D$ Where: $F_L, F_I, F_D$ represent the load characteristic, installation method, and soil density, respectively; the values are all 1.0 in this paper.	Long and Vanneste (1994)
LM1	$y_N = y_1(1 + t \cdot \ln N)$ $t = 0.18 \times (\Delta F/F_{\max})$ Where: $t = 0.18 \times 0.3 = 0.054$ in this paper.	Verdure et al. (2003)
LM2	$y_N = y_1 \left[ 1 + t_b \cdot \ln\left(\frac{N}{2} + 1\right) \right]$ $t_b = 0.05 \times \frac{(N-1)}{N}$	Bienen et al. (2012)

## Conclusions

Three-dimensional numerical analyses are performed to investigate the lateral load bearing capacity and long term response of monopiles in dense sand. These monopiles with outer diameters of 6 m have various slenderness ratios and load eccentricities to study the effect of monopile geometry. The degradation stiffness model is adopted to simulate the long term response of the monopile, and the accumulated displacement of each monopile is analyzed. Models to predict the accumulated displacement of monopiles are evaluated and refined in this study. For monopiles subjected to one-way cyclic loading:

- Study on criteria for determination of ultimate capacity  $F_u$  of laterally loaded monopile shows that the capacities determined according to widely used  $y_0 = 0.1D$  and  $\theta_0 = 2^\circ$  agree well with each other, regardless of the monopile's slenderness ratio and load eccentricity. Therefore, this study recommended that the ultimate capacity  $F_u$  can be determined according to the lateral displacement of  $0.1D$  at the mudline.
- The maximum loading cycles needed to reach a plateau value of accumulated displacement is increased with load amplitude. Accumulated displacement cannot converged even after up to  $6 \times 10^5$  loading cycles with load amplitude parameter  $\zeta_b$  larger than a value, e.g.,  $\zeta_b = 0.69$  in this study.
- The rotation point is located around a depth of  $0.7L_{em}$  and it increases with the increasing of load cycle numbers, and is independent of the magnitude of applied load amplitudes.
- The most widely used logarithmic model and power model generally produce a good estimation of accumulated displacement of the monopile, even the logarithmic model gives under-estimation at higher load levels (i.e., corresponding to a larger value of  $\zeta_b$ ).

- For power model, the value of model constants  $\alpha$  not only depends on the maximum load in each cycle (i.e., load parameter  $\zeta_b$ ), but is also heavily related to the monopiles' slenderness ratio. Additionally, it is independent of load eccentricity. Once the monopile's embedded length reaches  $8L_{em}$ , the value of  $\alpha$  is only related to the maximum load in each cycle.
- The constant  $\alpha$  of power model increases lineally with load amplitude and decreases with the increasing of monopile embedded ratio  $L_{em}/D$  in general. However, the constant is nearly kept unchanged when the monopile embedded ratio is larger than 8. According to the numerical simulations, the value of the power model parameter is independent of the load eccentricity.
- It should be noted that uniform ground condition is adopted in this study, for layered ground or a ground with increased strength along the embedded length of the monopile, the findings in this study need be further studied.

**Acknowledgements** The authors acknowledge the funding received from National Natural Science Foundation of China (Grant No. 41372274 and No. 41502273) and from Program for Young Excellent Talents in Tongji University (Grant No. 2015KJ009) for supporting this research.

## References

- Achmus M, Kuo Y-S, Abdel-Rahman K (2009) Behavior of monopile foundations under cyclic lateral load. *Comput Geotech* 36(5):725–735
- Ahmed SS, Hawlader B (2016) Numerical analysis of large-diameter monopiles in dense sand supporting offshore wind turbines. *Int J Geomech* 16(5):04016018
- API (2011) Geotechnical and foundation design considerations, ANSI/API RP 2GEO, 1st edn. American Petroleum Institute Publishing Services, Washington
- Bienen B, Duhrop J, Grabe J, Randolph MF, White DJ (2012) Response of piles with wings to monotonic and cyclic lateral loading in sand. *J Geotech Geoenviron* 138(3):364–375
- Bolton MD (1986) The strength and dilatancy of sands. *Geotechnique* 36(1):65–78
- Carswell W, Arwade SR, DeGroot DJ, Myers AT (2016) Natural frequency degradation and permanent accumulated rotation for offshore wind turbine monopiles in clay. *Renew Energy* 97:319–330
- Depina I, Hue Le TM, Eiksund G, Benz T (2015) Behavior of cyclically loaded monopile foundations for offshore wind turbines in heterogeneous sands. *Comput Geotech* 65:266–277
- Dewaikar DM, Padmavathi SV, Salimath RS (2008) Ultimate lateral load of a pile in soft clay under cyclic loading. *Proc 12th IACMAG: Geomechanics in the Emerging Social & Technological Age*, 1–6 October 2008, Goa, India, pp 3498–3507
- DNV (2014) DNV-OS-J101: Design of offshore wind turbine structures. Det Norske Veritas, Oslo
- Garnier J (2013) Advances in lateral cyclic pile design: contribution of the SOLCYP project. In Puech A: *Proc TC 209 Workshop 18th ICSMGE-Design for cyclic loading: piles and other foundations*. Paris, pp 59–68

- Huurman M (1996) Development of traffic induced permanent strain in concrete block pavements. *Heron* 41(1):29–52
- Kirwan L (2015) Investigation into ageing mechanisms for axially loaded piles driven in sand. Dissertation, University College, Dublin
- Klinkvort RT, Hededal O (2013) Lateral response of monopile supporting an offshore wind turbine. *Proc ICE - Geotech Eng* 166(2):147–158
- Klinkvort RT, Hededal O (2014) Effect of load eccentricity and stress level on monopile support for offshore wind turbines. *Can Geotech J* 51(9):966–974
- Kuo Y, Achmus M, Abdel-Rahman K (2012) Minimum embedded length of cyclic horizontally loaded monopiles. *J Geotech Geoenviron* 138(3):357–363
- Leblanc C, Houlsby GT, Byrne BW (2010) Response of stiff piles in sand to long-term cyclic lateral loading. *Geotechnique* 60(2):79–90
- Li W, Gavin K, Doherty P (2013) Experimental investigation on the lateral load capacity of monopiles in dense sand. *Proc 38th Annual Conference on Deep Foundations*. Phoenix, AZ, pp 67–75
- Li W, Igoe D, Gavin K (2015) Field tests to investigate the cyclic response of monopiles in sand. *Proc ICE-Geotech Eng* 168(GE5):407–421
- Li W, Zhu B, Yang M (2017) Static response of monopile to lateral load in over-consolidated dense sand. *J Geotech Geoenviron*. 143(7): 04017026. doi:10.1061/(ASCE)GT.1943-5606.0001698
- Little RL, Briaud J-L (1988) Full scale cyclic lateral load tests on six single piles in sands. Texas A&M University, College Station
- Long JH, Vanneste G (1994) Effects of cyclic lateral loads on piles in sand. *J Geotech Eng* 120(1):225–244
- Peralta P (2010) Investigation on the behaviour of large diameter piles under long-term lateral cyclic loading in cohesionless soil. *Civil Engineering and Geodetic Science*. Dissertation, Leibniz University, Hannover
- Rajashree SS, Sundaravadivelu R (1996) Degradation model for one-way cyclic lateral load on piles in soft clay. *Comput Geotech* 19(4):289–300
- Randolph MF (1981) The response of flexible piles to lateral loading. *Geotechnique* 31(2):247–259
- Reese LC, Cox WR, Koop FD (1974) Analysis of laterally loaded piles in sand. *Offshore Technology in Civil Engineering Hall of Fame Papers from the Early Years*, pp 95–105
- Tolooiyan A, Gavin K (2011) Modelling the cone penetration test in sand using cavity expansion and arbitrary lagrangian eulerian finite element methods. *Comput Geotech* 38(4):482–490
- Verdure L, Garnier J, Levacher D (2003) Lateral cyclic loading of single piles in sand. *Int J Phys Model Geotech* 3(3):17–28
- Yang M, Ge B, Li W, Zhu B (2016) Dimension effect on P-y model used for design of laterally loaded piles. *Procedia Eng* 143:598–606
- Zdravković L, Taborda DMG, Potts DM et al. (2015) Numerical modelling of large diameter piles under lateral loading for offshore wind applications. *The Third International Symposium of Frontiers in Offshore Geotechnics (ISFOG2015)*. Oslo, Norway, pp 759–764